

Thermal junctions controlled with magnetic phases

José Balduque,¹ Adrián Mecha,¹ and Rafael Sánchez^{1,2,3}

¹*Departamento de Física Teórica de la Materia Condensada, Universidad Autónoma de Madrid, 28049 Madrid, Spain*

²*Condensed Matter Physics Center (IFIMAC), Universidad Autónoma de Madrid, 28049 Madrid, Spain*

³*Instituto Nicolás Cabrera, Universidad Autónoma de Madrid, 28049 Madrid, Spain*

(Dated: 10 May 2024)

Unlike charge, heat flows are difficult to control. We show that, in mesoscopic conductors, electronic thermal currents can be manipulated with a magnetic field by using the Aharonov-Bohm effect: the magnetic control of the interference pattern enhances the thermoelectric effect, while heat transport can be totally suppressed. In a three-terminal configuration, the flux-induced broken reciprocity generates a non-local thermoelectric response and translates to the circulation of heat. This way, efficient thermoelectric generators, thermal switches and thermal circulators, as well as energy harvesters can be defined for minimally disturbing thermal management at the nanoscale.

I. INTRODUCTION

Transport through mesoscopic conductors is determined by the phases that electrons accumulate in the different trajectories between terminals¹. In systems with several barriers², or in molecular junctions³, the interference of kinetic phases acquired during multiple reflections between two scattering regions result in Fabry-Pérot or Fano resonances. Trajectories enclosing a magnetic field acquire an additional phase which leads to the Aharonov-Bohm effect⁴. If the trajectories are confined in a quasi-one-dimensional ring, the current presents flux-dependent oscillations^{5,6} that can be controlled experimentally^{7,8} and revealed the nonlocal nature of quantum transport^{9,10}. They are a useful tool to measure magnetic asymmetries of the transport coefficients^{11–14} and fluctuations^{15,16}, measurement-induced dephasing^{17,18}, scattering phases^{19–32}, heat transport³³, or the coherence in topological states³⁴ and fractional excitations in the quantum Hall regime^{35,36}. The interplay of different such interferences may also arise in quantum dot structures^{37–45}.

The energy dependence of kinetic phases has motivated coherent conductors to be useful for thermoelectrics^{46–59}, as it naturally breaks electron-hole symmetry in an interferometer^{60–67}. In three terminal configurations^{68–73}, this property allows for the conversion of heat injected in a junction into electrical power, only relying on the properties of the junction⁶⁶, and in the absence of charge injection from the heat source. When the contact is given by a scanning probe^{65,66,74}, the heat source can be disconnected at will. However, one does not have such possibility in most experimental realizations, where the injection of heat is permanent and difficult to control.

For the development of nanoscale and quantum technologies, it would be desirable to achieve a similar degree of control of heat currents as for charge to manage the excess heat in such devices. While the control of charge currents is routinely done by external voltages, such a contact for heat is limited by the Joule and the Seebeck effects^{75–77}. Despite the formidable advances in the last years^{78–81}, this goal is still challenging, with few experimental demonstrations of thermal devices (thermal diodes or transistors) so far^{82–87}, especially in normal conductors^{88–90}. In particular, junctions that control noninvasively how heat is injected, such as thermal

switches^{63,91–93}, modulators⁹⁴ or circulators^{95–98}, would enhance the definition of integrated heat circuits^{99–101}. Single-electron transistors have been proposed^{102–104} which are restricted to very low powers.

Recently Haack *et al.* have proposed the Aharonov-Bohm effect as a mechanism to control both the thermoelectric response^{105–107} and the flow of heat in two-terminal ring conductors by using the magnetic field as a knob^{63,64,67}. Following these ideas, we investigate a minimal model of a multiterminal ring able to exploit the nonlocal features of the Aharonov-Bohm effect to be used as a thermoelectric engine, a thermal switch and a heat circulator, as illustrated in Fig. 1, furthermore allowing for an analytical description of the relevant processes in terms of the properties and symmetries of the transport coefficients. This is done based on three main properties: (i) The interplay of the kinetic and magnetic phases leading to an enhanced thermoelectric effect; (ii) the flux-dependent but energy-independent destructive interference of the Aharonov-Bohm scattering leading to the suppression of all (charge and heat) currents, hence to a heat switch

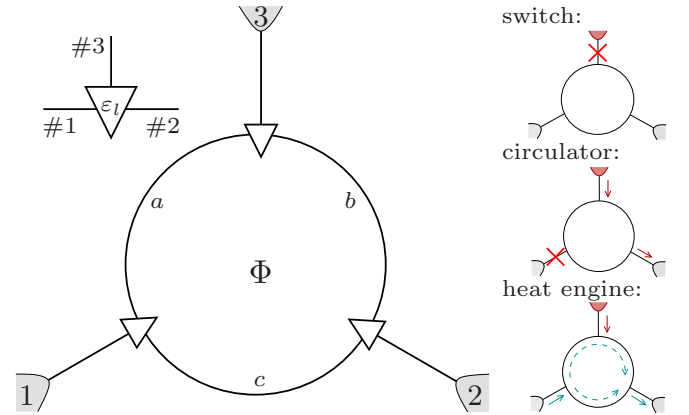


FIG. 1. Single-channel three-terminal quantum ring. Each terminal is in local equilibrium with an electrochemical potential μ_l and a temperature T_l ($l=1,2,3$) and coupled to the ring by a beam-splitter with coupling ε_l dividing the ring in three segments of length L_α ($\alpha=a,b,c$). A magnetic flux Φ pierces the ring inducing a magnetic phase $\pm\varphi_\alpha$ in the electrons propagating along each segment. Insets show the scheme for the ring-lead junctions and the three main operations considered here.

that avoids undesired thermoelectric effects, and (iii) the broken time reversal symmetry leading to asymmetric transport coefficients in multiterminal configurations and hence to thermal circulator and energy harvester^{68,69,108–116} effects. We pay special attention to the role of dephasing^{2,117,118} in two-terminal configurations and of nonreciprocal transport in three-terminal setups. We will focus on switches and circulators in *all-thermal* configurations i.e., imposing that no charge but only heat is injected from the different terminals by assuming open-circuit conditions, this way defining contactless onchip thermal devices tuned by flux. For comparison, we will also consider *electrothermal* cases which relax that condition by allowing charge to flow and facilitate a simple analytical treatment in limiting cases.

The remaining of the manuscript is organized as follows. In Sec. II we introduce the theoretical description of our model based on scattering theory. Sections III and IV present the results for two and three terminal configurations, respectively, with the conclusions being discussed in Sec. V.

II. SCATTERING THEORY

Before describing transport, it is useful to describe the states in the ring. Solving the Schrödinger equation for a single mode closed ring of circumference L pierced by a magnetic flux Φ yields a spectrum given by the eigenenergies¹¹⁹

$$\epsilon_n = U_r + \frac{2\pi^2\hbar^2}{mL^2} \left(n - \frac{\phi}{2\pi} \right)^2, \quad (1)$$

where U_r is the bottom of the confinement potential, $\phi = 2\pi\Phi/\Phi_0$ is the phase accumulated upon performing a loop around the ring, with $\Phi_0 = h/c$ being the flux quantum, and m the mass of the electron (see also Ref. 120).

When connected to leads, the states of the ring mediate the transmission of electrons through the conductor terminals⁶. We will consider here two and three terminal configurations. The most general case is sketched in Fig. 1. It is decomposed in three connected three-channel junctions treated as beam-splitters. For simplicity, we assume that the transmission from the terminal channels into the ring ones is symmetric, leading to a scattering matrix⁶:

$$S_{\alpha l}^{\nabla} = \begin{pmatrix} -e^{i\chi_{\alpha}}\eta_l^{-}/2 & e^{i\varphi_{\alpha}^{+}}\eta_l^{+}/2 & e^{i\varphi_{\alpha}^{+}}\sqrt{\epsilon_l} \\ e^{i\varphi_{\alpha}^{-}}\eta_l^{+}/2 & -\eta_l^{-}/2 & \sqrt{\epsilon_l} \\ e^{i\varphi_{\alpha}^{-}}\sqrt{\epsilon_l} & \sqrt{\epsilon_l} & \eta_l^{-}-1 \end{pmatrix} \quad (2)$$

for each junction, with the elements ordered as in the inset of Fig. 1. The phases $\varphi_{\alpha}^{\pm} = \chi_{\alpha} \pm \phi_{\alpha}$ accumulated by the waves in the segment $\alpha \in \{a, b, c\}$ when propagating clock- (+) or anticlockwise (-) contain a kinetic, $\chi_{\alpha} = \sqrt{2m(E - U_0 - eV_{g,\alpha})}L_{\alpha}/\hbar$, where U_0 is the energy of the lowest ring sub-band, and a magnetic part, ϕ_{α} , both depending on the length of the segment L_{α} . They can be tuned by means of the voltage $V_{g,\alpha}$ applied to plunger gates, or of the magnetic phase, $\phi = \sum_{\alpha} \phi_{\alpha}$. It is convenient to invoke gauge

invariance and accumulate the magnetic phase in a single segment, e.g. $\phi_a = \phi$, $\phi_b = \phi_c = 0$. The coupling between terminal $l \in \{1, 2, 3\}$ and the ring is given by $\epsilon_l \in [0, 1/2]$, which is used to define $\eta_l^{\pm} = 1 \pm \sqrt{1 - 2\epsilon_l}$. The two-terminal configuration is trivially obtained from this by simply setting $\epsilon_3 = 0$ and $L_c = 0$. In what follows, and in order to emphasize the asymmetries introduced by the phases, we will consider symmetric configurations, with all nonvanishing couplings and lengths being equal, $\epsilon_l = \epsilon$ and $L_{\alpha} = L/N$, with $N = 2, 3$ being the number of terminals, and the couplings to be energy independent. Also, lengths will be expressed in units of $l_0 = 2\pi\hbar/\sqrt{2mk_B T}$, which for GaAs rings is of the order of 730 nm at $T = 1$ K.

With these matrices, one obtains the scattering matrix $S_{l'l}(E)$ of the whole conductor by identifying the outgoing waves of a junction with the ingoing ones of the next one along the ring. The procedure is detailed in textbooks¹²¹, see also Ref. 66. A relevant quantity for transport will be the difference $\mu - U_r$ set by the equilibrium chemical potential of the terminals and the overall potential $U_r \equiv U_0 + eV_g$: it determines the kinetic phase of the electrons scattered at the Fermi energy. We will for simplicity chose $\mu = 0$ as a reference energy and modulate U_r with a gate voltage globally acting on the ring in the following results. Different from Ref. 63, we will furthermore ignore asymmetries induced by the gate voltages setting $V_g \equiv V_{g,\alpha}$, and consider only the effect of the ring potential U_r .

A. Transport

With the scattering matrix of the system, $S_{l'l}(E)$, we write the charge and heat currents¹²²:

$$I_l = \int_{-U_r}^{\infty} dE i_l(E) \quad \text{and} \quad J_l = \int_{-U_r}^{\infty} dE (E - \mu_l) i_l(E), \quad (3)$$

in terms of the spectral currents:

$$i_l(E) = \frac{2}{h} \sum_{l'} \mathcal{T}_{l'l}(E) [f_l(E) - f_{l'}(E)], \quad (4)$$

where $\mathcal{T}_{l'l}(E) = |S_{l'l}(E)|^2$ is the transmission probability for an electron injected from terminal l to be absorbed by terminal l' , and $f_l(E) = \{1 + \exp[(E - \mu_l)/k_B T_l]\}^{-1}$ is the Fermi distribution function of terminal l having an electrochemical potential μ_l and a temperature T_l ; the factor 2 accounts for spin degeneracy. Both particle and heat currents are defined as positive when emitted by a reservoir. In the presence of a magnetic field, the scattering matrix becomes asymmetric, with reciprocity being expressed as $S_{l'l}(\Phi) = S_{l'l}(-\Phi)$ ¹², a property that affects the inelastic thermopower^{70,123,124} and that we will exploit in multiterminal configurations.

Scattering theory guarantees charge and energy conservation: $\sum_l I_l = 0$ and $\sum_l (J_l + \mu_l I_l) = 0$. The second term in the later equation corresponds to power dissipated as Joule heating. For the thermoelectric engine, we define the power output

$$P = \Delta\mu I_1, \quad (5)$$

with $\Delta\mu = \mu_2 - \mu_1$ so that it is positive when generated from the conversion of heat: electrons flow from lower to higher electrochemical potential terminals.

B. Open-circuit condition

Occasionally, we will require that some terminals inject heat but no charge, on average, into the conductor. This will be the case of the all-thermal operations and of the heat source of the three-terminal energy harvester. This is done by assuming an open circuit condition, such that the chemical potential of the involved terminals develops to a value μ_l that maintains a vanishing charge current. We then need to solve the equations $I_l(\mu_l) = 0$ for those terminals.

C. Dephasing

To evaluate the effect of decoherence in scattering theory, one introduces fictitious terminals which absorb and reinject electrons with the same energy but a randomized phase^{2,117,118}. In order to do so without introducing additional interference, the dephasing probe terminals need two channels coupled to the conductor via scattering matrices of the type¹¹⁷

$$S_\alpha^\diamond = \begin{pmatrix} 0 & \sqrt{1-\lambda_\alpha} & \sqrt{\lambda_\alpha} & 0 \\ \sqrt{1-\lambda_\alpha} & 0 & 0 & \sqrt{\lambda_\alpha} \\ \sqrt{\lambda_\alpha} & 0 & 0 & -\sqrt{1-\lambda_\alpha} \\ 0 & \sqrt{\lambda_\alpha} & -\sqrt{1-\lambda_\alpha} & 0 \end{pmatrix}, \quad (6)$$

where $\lambda_\alpha \in [0, 1]$ parametrizes the coupling of the probe to segment α of the ring. We are avoiding here the introduction of additional (and unnecessary) phases. To satisfy that the spectral current $i_\alpha(E)$ vanishes, i.e.:

$$\sum_l \mathcal{T}_{l\alpha}(E)[\tilde{f}_\alpha(E) - f_l(E)] = 0, \quad (7)$$

where l includes all other terminals (fictitious or not), one needs to impose the condition that the probe has a nonthermal distribution $\tilde{f}_\alpha(E)$ that solves Eq. 7 for each energy. In the two-terminal setup, we will restrict to the case where each segment is coupled to a different dephasing probe with equal strength $\lambda_\alpha = \lambda$. In the three-terminal setup, we will for simplicity assume that $\lambda_a = \lambda = 0$ and only $\lambda_c = \lambda$ can be finite.

III. TWO TERMINALS

We start with the two-terminal configuration, which has been shown to work as a thermoelectric engine and switch^{63,64}. In this configuration, we set $\varepsilon_3 = 0$ and $L_c = 0$ in the scheme of Fig. 1. In the transmission probability through the quantum ring in that configuration and in the absence of dephasing ($\lambda = 0$)^{6,63}

$$\mathcal{T}_{12}^{(2t)}(E) = \frac{8\varepsilon^2 \sin^2 \chi (1 + \cos \phi)}{4\varepsilon^2 \sin^2 \tilde{\chi} + [(\varepsilon - \eta^+) \cos \phi + 2(1 - \varepsilon) \cos \tilde{\chi}]^2}, \quad (8)$$

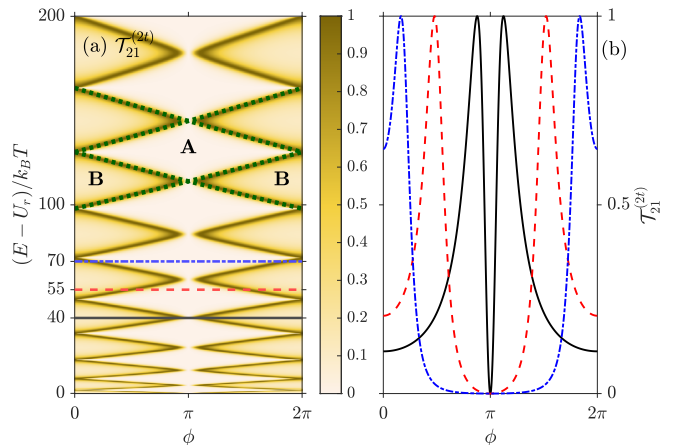


FIG. 2. Two terminal transmission probability (a) as a function of energy and the magnetic phase, for a ring of circumference $L = l_0/2$ with $\varepsilon = 0.25$. Dotted green lines mark the energy of the closed ring eigenvalues ϵ_n for $n = -4, \pm 5, 6$. (b) Cuts of the previous at the energies marked by the lines with the corresponding linestyle: $E - U_r = 40k_B T, 55k_B T, 70k_B T$.

with $\tilde{\chi} = \chi_a + \chi_b$, one sees two contributions to the interference pattern. The transmission oscillates both via ϕ , which is tuned with the magnetic flux, and via the kinetic phases χ_α , which depend on the circumference of the ring and on energy and therefore can be controlled by the potential U_r , as shown in Fig. 2. Note that in the symmetric case we are considering, $\mathcal{T}_{12}^{(2t)}(E) \propto 1 + \cos \phi$, hence total destructive interference occurs at odd multiples of $\phi = \pi$, irrespective of μ . In less symmetric configurations, this condition depends on χ_a and χ_b .

We distinguish two kinds of diamond-shaped regions in the ϕ -dependence of the transmission, separated by resonances at $E = \epsilon_n$, cf. Fig. 2(a): around odd multiples of π , labeled as A in Fig. 2(a), destructive interference suppresses the transmission probability, which is exactly cancelled at $\phi = (2n + 1)\pi$. The resonances hence do not cross each other at the crossings of the eigenstates there. Differently, states crossing at even multiples of 2π interfere constructively. In those regions, labelled as B in Fig. 2(a), the transmission is not totally suppressed between peaks. Note that the shape of the resonances depends on the magnetic flux⁶, see Fig. 2(b). This property has consequences for the thermoelectric performance, as discussed below. At energies corresponding to a single eigenmode, asymmetric single resonances appear, which can be used as filters for efficient heat to charge conversion¹²⁵. Differently, close to the crossing of two eigenmodes double-peaked resonances develop, with sharper tails, which are promising candidates for power improving thermoelectrics¹²⁶, see also Ref. 127. The dependence on energy is also interesting as the quadratic dependence in Eq. (1) increases the separation between resonances with increasing n . This is to be taken into account for the thermoelectric response, as typically it increases when broken electron-hole symmetry is resolved within the range of thermal fluctuations. Hence, depending on the scale $k_B T$, the ring potential can be

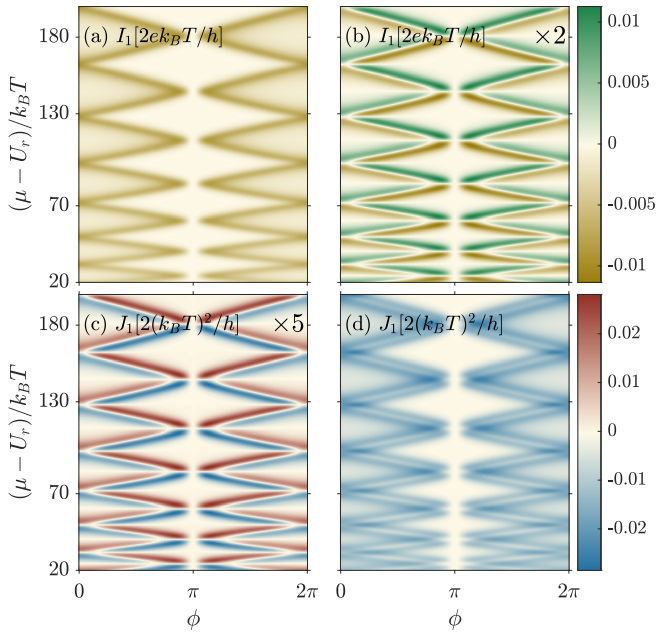


FIG. 3. Charge, I , and heat, J , currents as functions of the magnetic phase and the chemical potential for $L = l_0/2$ and $\varepsilon = 0.25$, with (a),(c) $\Delta\mu = 0.01k_B T$ and $\Delta T = 0$, and (b),(d) $\Delta T/T = 0.01$ and $\Delta\mu = 0$.

adjusted to enhance the response: higher temperatures require high enough $\mu - U_r$.

Charge and heat currents are shown in Fig. 3 for finite and small chemical potential and temperature differences ($T_1 = T$, $T_2 = T + \Delta T$, $\mu_1 = \mu + \Delta\mu/2$, $\mu_2 = \mu - \Delta\mu/2$) for a ring of circumference $L = l_0/2$. Following the transmission in Fig. 2, currents are 2π -periodic in ϕ and show diamond-shaped regions around $\phi = \pi$ where transport is suppressed by destructive interference. Notably, at $\phi = \pi$, both charge and heat currents are exactly cancelled, as $\mathcal{T}_{12}^{(2r)}(E) = 0$ for all energies. As for the transmissions, the current peaks tend to separate with $\mu - U_r$. As we are considering relatively low temperatures, all resonances are clearly resolved.

As can be seen in Figs. 3(b) and 3(c), the sharp spectral features of the transmission induce a thermoelectric response. This manifests in the form of a Seebeck heat to charge converter when the two terminals support a temperature difference ΔT , cf. Fig. 3(b), and of Peltier cooling in the presence of a small electrochemical potential difference, $\Delta\mu$, cf. Fig. 3(c). In both cases, the current changes sign around the transmission peaks, as expected for sharp resonances as those occurring in e.g., quantum dots^{128–134}. As we are considering small differences within the linear regime, $\Delta\mu, \Delta T \ll k_B T$, the two effects show similar features, as corresponds from the Onsager reciprocity relations¹³. Note that in a two terminal geometry, linear transport coefficients are even functions of the magnetic field, see also Eq. (8).

Let us now consider the effect of dephasing by coupling each segment to a dephasing probe with equal strength $\lambda_\alpha = \lambda$. By increasing the coupling, additional trajectories contribute where the electrons lose their phase before being ab-

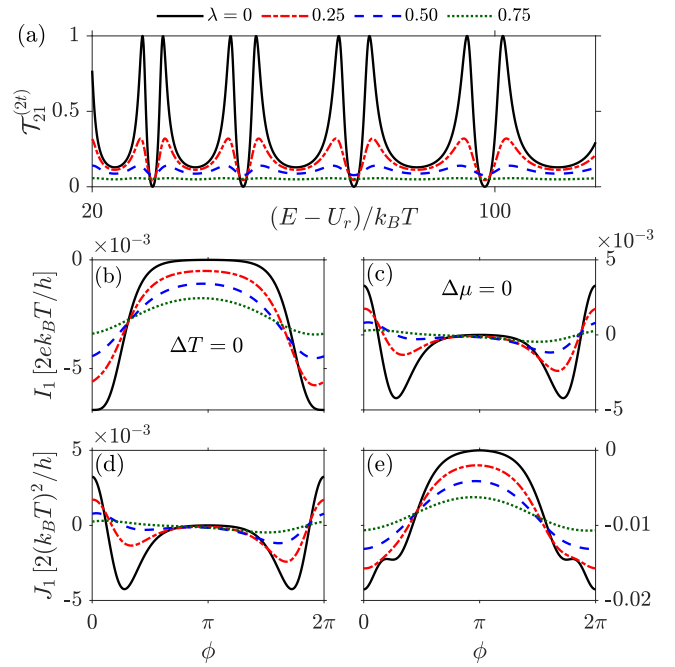


FIG. 4. Effect of dephasing. (a) Two terminal transmission probability as a function of energy for $\mu - U_r = 100k_B T$ and $\phi = \pi/4$, and (b),(c) charge and (d),(e) heat currents as functions of the magnetic flux, for different couplings to the dephasing probes, with (b),(d) $\Delta T = 0$ and $\Delta\mu = 0.01$ and (c),(e) $\Delta T/T = 0.01$ and $\Delta\mu = 0$. The magnetic field dependent oscillations disappear with the coupling to the probes, as expected. Other parameters: $\varepsilon = 0.25$, $L = l_0/2$

sorbed by one of the transport terminals (1 and 2). These are not affected by interference, hence reducing the resonances, cf. Fig. 4(a). As dephasing increases, the role of the kinetic and magnetic phases is suppressed and the oscillations get increasingly flattened. In the strong dephasing limit $\lambda = 1$, all injected electrons are absorbed by the dephasing probes and reinjected with a randomized phase (hence $\mathcal{T}_{21}^{(2r)}(E) = 0$) so transport is fully incoherent. The impact on the currents is shown in Figs. 4(b)-(e). The flux dependence of the charge and thermal conductances is washed out and stays finite, as expected from an incoherent conductor, see Figs. 4(b) and (e). The thermoelectric response is however suppressed for any value of the flux, see Fig. 4(b), confirming that the thermoelectric response relies on the broken electron-hole symmetry induced by the kinetic phases⁶⁶.

A. Thermoelectric generator

Let us evaluate the performance of the thermoelectric effect by the generated power and the efficiency $\eta = P/J_1$. We do this in Figs. 5(a) and 5(b) for different couplings ε and comparing to the thermodynamic bounds given by the Carnot efficiency $\eta_C = \Delta T/(T + \Delta T)$ and the Whitney-Pendry bound for the maximal power output from a single quantum channel^{126,135}, $P_W = 2A_0\pi^2\Delta T^2$, with $A_0 = 0.0321$. Weakly coupled rings generate small power outputs at a high efficiency⁶³

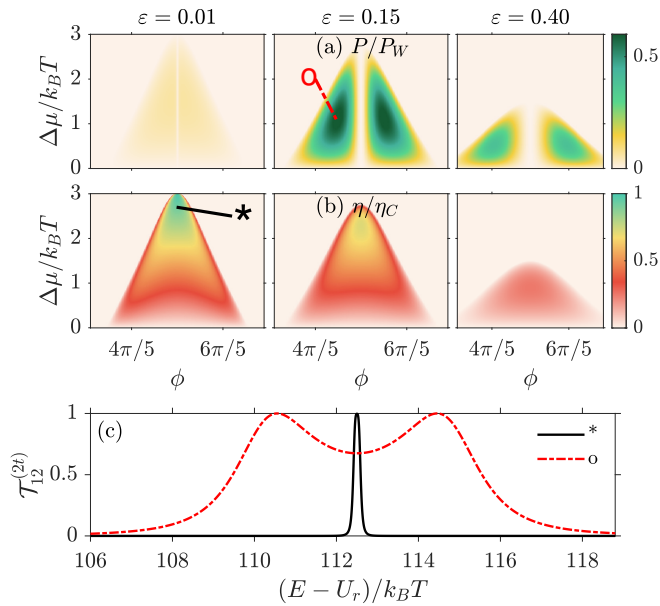


FIG. 5. (a) Power and (b) efficiency for $\varepsilon = 0.01$ (left), 0.25 (center) and 0.40 (right column). Parameters: $L = l_0/2$, $\mu - U_r = 108 k_B T$, $\Delta T/T = 1$. At low couplings, the low generated power is compensated by an efficiency close to Carnot's. While the efficiency decreases with ε , the power is maximal for intermediate couplings. (c) Transmission probability for the configurations corresponding to the maximal power P_{max} (red dashed, $\phi = 2.82$) and maximal efficiency η_{max} (black full line, $\phi = 3.132$) for the conditions indicated.

close to η_C . This occurs when a circulating state enters the transport window (defined by $\mu \pm 2k_B(T + \Delta T)$), leading to a very narrow resonance which is known to result in high efficiencies¹²⁵. The width of the resonance depends on the coupling to the leads. Hence, increasing ε affects the energy filtering and, as a consequence, the efficiency is reduced to a few tenths of η_C .

The effect of coupling to the power is two-fold: on one hand, broad resonances allow for larger currents contributing to more power; on the other hand, energy resolution in filtering is lost, which harms the thermoelectric effect. A compromise is found at intermediate couplings where power is maximal, around $0.6P_W$, and efficiency is still around $\eta_C/2$, see Fig. 5(a) and 5(b). The large power output can in this case also be attributed to the spectral properties of the ring: enabled by a sufficiently large ε , the overlap of two resonances occurring close to the crossing of the ring states result in a broad double peak whose tails are sharpened by the destructive interference, see Fig. 5(c), a property that has been discussed to optimize the power output^{74,126,127,136}. Remarkably, the position of the resonances is the same both for obtaining a maximal power and a maximal efficiency.

The compromise between power and efficiency is further explored in Fig. 6, which shows their mutual values as voltage is tuned from zero to the stall voltage where I vanishes, and compared to the maximal value P_{max} for a given efficiency obtained by a boxcar transmission¹²⁶. We do this in the two optimal configurations of Fig. 5. It is found that the low cou-

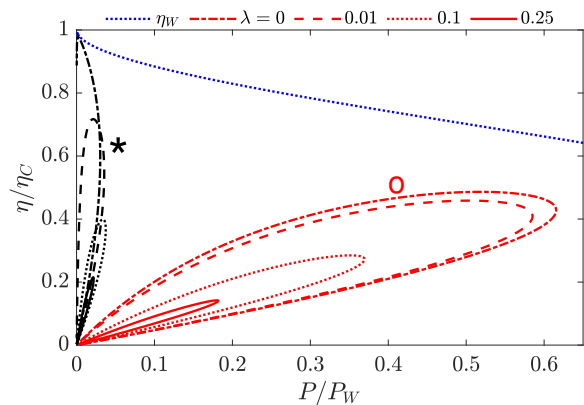


FIG. 6. Loop diagrams for efficiency vs. power for the optimal configurations considered in Fig. 5(c) giving P_{max} (red) and near η_{max} (black). The effect of dephasing is shown by varying the coupling to the dephasing probes, λ . Parameters that are not indicated in the figure are as in Fig. 5.

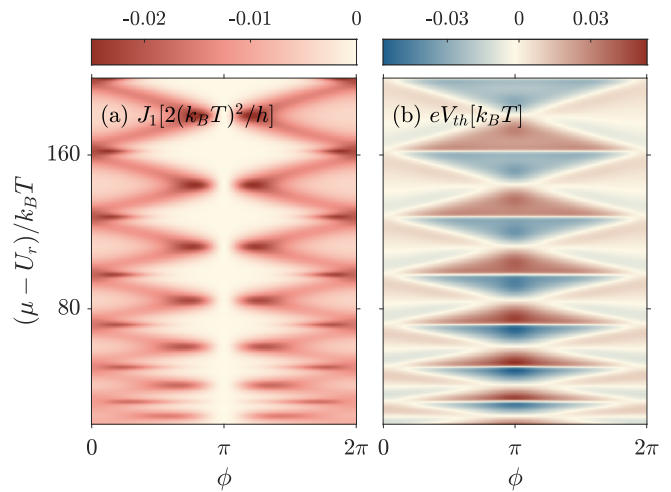


FIG. 7. (a) Heat current in the two terminal all-thermal configuration as a function of the tunable parameters: the magnetic flux and the ring potential. Tuning ϕ the system works as a thermal switch operating between a resonant transmission and a full cancellation of the current at $\phi = \pi$ for every value of U_r . Here, $\varepsilon = 0.25$ and $L = l_0/2$. (b) Thermovoltage $eV_{th} = \mu_2 - \mu_1$ developed to satisfy the condition $I_l = 0$ ⁶³.

pling case approaches both bounds η_C and P_{max} . However this result is very sensitive to dephasing. Optimizing power seems to be more robust: the case $\varepsilon = 0.15$ maintains large power outputs (though far from the bound P_{max}) in the presence of dephasing, with efficiencies comparable to the case $\varepsilon = 0.01$ for the same λ .

B. All-thermal switch

The transport properties shown in Fig. 3 can be used as a switching mechanism⁶³: by simply sweeping the magnetic

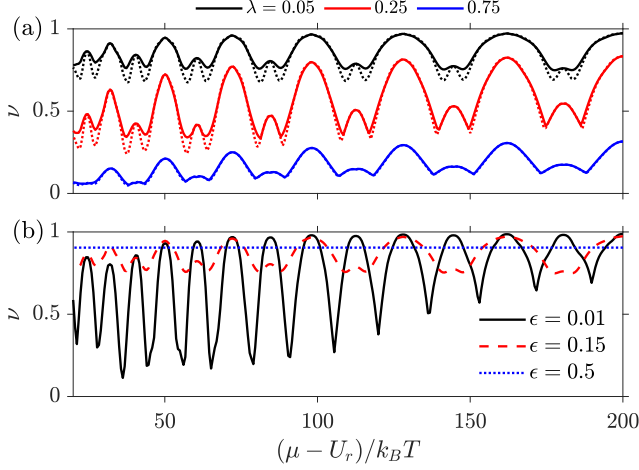


FIG. 8. Two terminal switch coefficient as a function of the ring potential (a) for $\epsilon = 0.25$ and $L = l_0/2$, for increasing coupling to the dephasing probes, $\lambda = \lambda_\alpha$, and (b) for $\lambda = 0.05$ and different ϵ , with otherwise similar parameters ($\Delta T/T = 0.01$, $\Delta\mu = 0$).

field, one changes the device from a resonantly conducting to an insulating state, both for charge and for heat currents. We are interested here in the later ones, and indeed assume the all-thermal condition where the charge current vanishes by considering an open conductor configuration. The two terminals then develop a chemical potential difference which coincides with the thermovoltage $\mu_2 - \mu_1 = eV_{th}$, plotted in Fig. 7 with the resulting heat current. By comparing Figs. 3(d) and 7(a) one appreciates that the heat current is different in the short and open circuit configurations. In particular, double peaks in Figs. 3(d) merge into wide single-featured resonances in Fig. 7(a) as the potential is tuned, and the double-peak resonances around even multiples of $\phi = \pi$ become considerably wider and extend into the negative-interference regions in the open circuit case. Of course, also in open circuit all currents vanish at $\phi = \pi$.

We parameterize the switching operation by the visibility of the thermal interference pattern as a function of the magnetic flux for all other parameters fixed:

$$v(\phi) = \frac{J_{max}(\phi) - J_{min}(\phi)}{J_{max}(\phi) + J_{min}(\phi)}, \quad (9)$$

which is 1 if the current is totally blocked. In the case $\lambda = 0$, the full destructive interference leads to $v = 1$ at any condition. For finite coupling to the dephasing probes, the switch coefficient becomes parameter-dependent and $v < 1$, see Fig. 8(a). However, for low λ the visibility can be tuned to still approach 1, especially for low coupling to the leads $\epsilon \ll 1/2$ and increasing $\mu - U_r$, as shown in Fig. 8(b).

In Fig. 8(a) we compare the all-thermal (solid) and electro-thermal (dotted lines) switching. The two cases have similar maxima, however, the all-thermal switching is more stable under the variation of the chemical potential. The two cases become indistinguishable as dephasing increases.

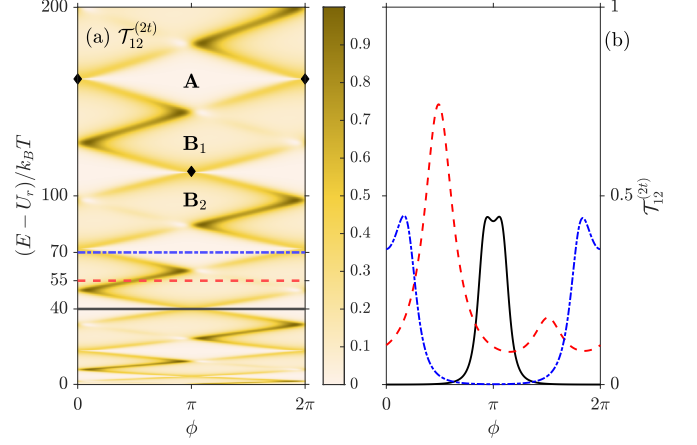


FIG. 9. Three-terminal transmission probability between clockwise connected terminals, $\mathcal{T}_{12}(E, \phi) = \mathcal{T}_{\bar{1}2}(E, \phi) = \mathcal{T}_{\bar{1}2}(E, -\phi)$, (a) as a function of energy and the magnetic phase, for a ring of circumference $L = l_0/2$ with $\epsilon = 0.25$. (b) Cuts of the previous at the energies marked by the lines with the corresponding linestyles: $E - U_r = 40k_B T, 55k_B T, 70k_B T$.

IV. THREE TERMINALS

We now extend the configuration to include a third terminal, as sketched in Fig. 1. We recall that we are assuming a symmetric configuration, with equidistantly separated junctions ($L_\alpha = L/3$) and equally coupled ($\epsilon_l = \epsilon$). This way, the necessary asymmetries involved in the proposed operations can only be attributed to the magnetic field induced asymmetry of the Onsager-Casimir reciprocity relations, $\mathcal{T}_{ij}(\Phi) = \mathcal{T}_{ji}(-\Phi)$, which only play a role in multiterminal systems. Furthermore in our case, we can express it in terms of a single transmission coefficient, $\mathcal{T}_{\bar{1}2}(\Phi) = \mathcal{T}_{12}(\phi) = \mathcal{T}_{23}(\phi) = \mathcal{T}_{31}(\phi) = |\mathcal{A}|^2$, with the transmission amplitude $\mathcal{A} = \mathcal{N}/\mathcal{D}$ and

$$\begin{aligned} \mathcal{N} &= 16i\epsilon e^{i2\chi} \sin \chi \left[2e^{-i\chi} + e^{-i\phi} \eta_+ + 2e^{i(\chi+\phi)}(\eta_+ - 1) \right] \\ \mathcal{D} &= -16e^{-i\chi} + 12e^{i\chi} \eta_-^2 + 4e^{i2\chi} \cos \phi \eta_+^3 \\ &\quad - 3e^{i\chi} \eta_-^2 (\eta_-^2 - \eta_+^2) + e^{i5\chi} (\eta_-^2 - \eta_+^2)^3 / 4, \end{aligned} \quad (10)$$

plotted in Fig. 9. Here, $\chi = \chi_\alpha$. The other transmission probabilities are $\mathcal{T}_{\bar{1}2}(\phi) = \mathcal{T}_{21}(\phi) = \mathcal{T}_{32}(\phi) = \mathcal{T}_{13}(\phi) = \mathcal{T}_{\bar{1}2}(-\phi)$. It is useful to write it in the weak coupling limit ($\epsilon \rightarrow 0$):

$$\mathcal{T}_{\bar{1}2}^w = 2\epsilon^2 \sin^2 \chi \frac{[1 + \cos(2\chi)](1 + \cos \phi) - \sin(2\chi) \sin \phi}{\sin^2(3\chi) + 64 \cos^2 \phi}, \quad (11)$$

which gives a magnetoasymmetry $\delta\mathcal{T} = \mathcal{T}_{\bar{1}2} - \mathcal{T}_{\bar{1}2} \propto \sin \phi$ that changes sign around even multiples of $\phi = \pi$. Also $\mathcal{T}_{\bar{1}2}^w(\phi = (2n+1)\pi) = 0$. This is enough to break inversion symmetry when heat is injected from one terminal, so it will flow preferentially into one of the other terminals, resulting on a circulator. It can also be used to induce a directed charge current between the other terminals, resulting in an energy harvester. Both effects are discussed below. In the opposite (strongly

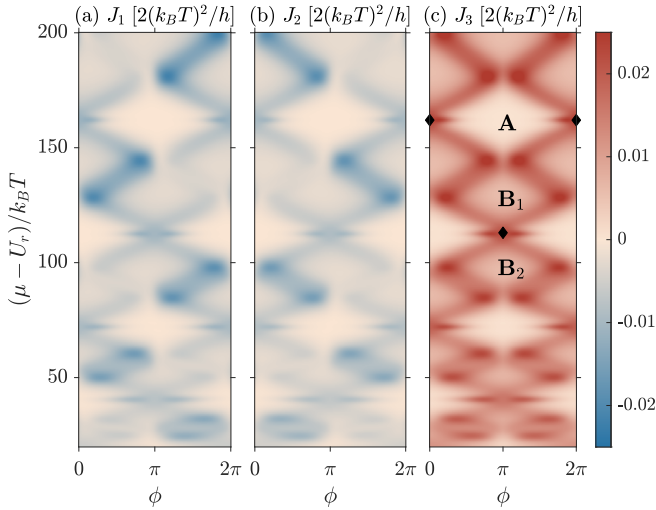


FIG. 10. Heat currents as functions of the magnetic phase and the ring potential for the case where all terminals inject no charge, $I_l = 0$, when terminal 3 is hot. Parameters: $\epsilon = 0.25$, $L = l_0/2$, $\Delta T/T = 0.01$.

coupled) limit, $\epsilon = 1/2$, we get

$$\mathcal{T}_3^s = 16 \sin^2(2\chi) [16 + \cos(\chi - \phi)] / D, \quad (12)$$

with the denominator D being an even function of ϕ . Also in this case, $\delta\mathcal{T} \propto \sin\phi$.

A. Heat currents

In the discussion below, terminal 3 will serve as a heat source for being at an increased temperature, $T_3 = T + \Delta T$, while terminals 1 and 2 remain at temperature T . The heat current J_3 is split into terminals 1 and 2, as shown in Fig. 10, where we have imposed that all reservoirs are voltage probes, such that their chemical potentials satisfy $I_l = 0$ (open circuit).

We readily see that destructive interference in the ring yields regions where all currents vanish. Therefore the switch effect is also present in a three terminal geometry. However, differently from the two-terminal case, the perfect suppression is limited by the interplay of the Aharonov-Bohm and the kinetic phases, cf. Eq. (10), so it does not occur for every electron density, in general. Interestingly, we find a regular sequence of three diamond-shaped regions centered around $\phi = \pi$, one of them insulating, labeled as A in Figs. 9(a) and 10(c), and the other two conducting, labeled as B₁ and B₂. We attribute this periodicity to the phase accumulated between terminals 1 and 2 being one third of the total phase $\sum_\alpha \chi_\alpha$ accumulated around the loop, which avoids the perfectly destructive interference except for some conditions determined by the ring potential (e.g., in the center of one every three diamonds)¹³⁷. Enhanced injection spots occur in the connection of two conducting regions, indicated with diamond shaped markers in Figs. 9(a) and 10(c), both at even and at odd multiples of $\phi = \pi$. At these spots, the current is equally absorbed by the other two terminals.

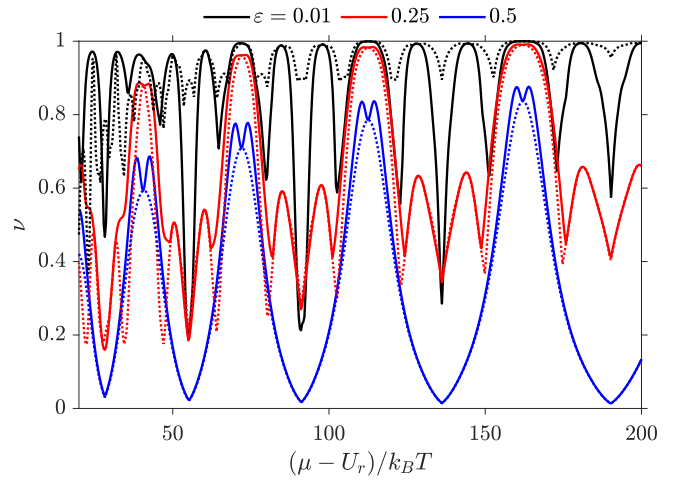


FIG. 11. Three-terminal heat switch effect as a function of the ring potential with $L = l_0/2$ for different couplings. Full lines: all-thermal, dotted: electrothermal (with $\Delta\mu = 0$). Parameters: $\Delta T/T = 0.01$, $\lambda = 0$.

We show the switching parameter ν of J_3 as a function of the ring potential for different couplings in Fig. 11. We find a doubly periodic behaviour predicted for non-negligible couplings which is less evident in the weak and strongly coupled regimes. In the tunneling regime with $\epsilon \ll 1$, the switch is most effective and tends to $\nu = 1$. Optimal values are also obtained for intermediate couplings for sufficiently high $\mu - U_r$.

We get an analytical understanding by comparing this behaviour with the electrothermal configuration (with all terminals having the same chemical potential, μ , dotted lines in Fig. 11), which shows similar properties in most cases, but is less affected by the χ -dependent oscillations at small ϵ . As terminals 1 and 2 are in the same equilibrium state (with the same temperature and chemical potential), described with the Fermi function f_{eq} , the integrand of J_3 is proportional to the spectral current $i_3 = (2/h)[\mathcal{T}_\zeta(\phi) + \mathcal{T}_\zeta(-\phi)](f_3 - f_{eq})$. In the limit $\epsilon \rightarrow 0$, we use Eq. (11) to find $i_3 \propto \sin^2\chi[1 + \cos(2\chi)](1 + \cos\phi)$, i.e. it vanishes at $\phi = \pi$, resulting in $\nu \rightarrow 1$, in agreement with Fig. 11. In the strongly coupled ring, $\epsilon \rightarrow 1/2$, from Eq. (12) we find $i_3 \propto \sin^2\chi(16 + \cos\chi\cos\phi)$, which describes the π -periodic in χ vanishing of ν . In this case, ϕ is not able to totally cancel the current, thus $\nu < 1$. However, one can use the kinetic phase to define a switch by tuning $\mu - U_r$ for constant ϕ . At intermediate couplings, the double periodic dependence can be explained by the injected electrons accumulating two different phases (either χ or 2χ) before they are absorbed.

B. Circulator

The finite magnetoasymmetry $\delta\mathcal{T}$ involves that $\mathcal{T}_{13} \neq \mathcal{T}_{23}$, i.e., electrons injected from terminal 3 will have a preferred terminal to be absorbed, despite they being in a similar thermodynamic state and the conductor being perfectly symmet-

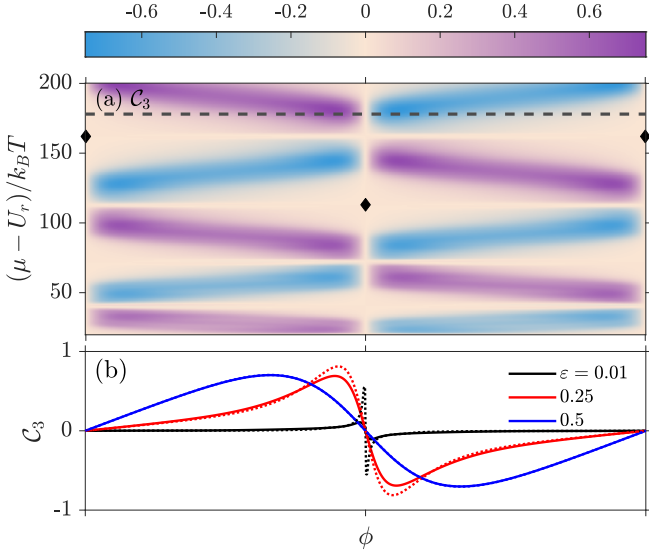


FIG. 12. (a) All-thermal circulation coefficient as a function of ϕ and the ring potential for $\varepsilon=0.25$ and $L=l_0/2$, with $\Delta T=0.01$. (b) Cuts for $(\mu - U_r)/k_B T = 177$ (solid line in (a)) and various couplings for the all-thermal (full lines) and the electrothermal (dotted) configurations.

ric (spatially). One already sees in Fig. 10 that $J_1(\phi) \neq J_2(\phi)$, but rather $J_1(\phi) = J_2(-\phi)$. We therefore define a circulation coefficient that measures this effect, considering that heat is injected from terminal 3, as

$$\mathcal{C}_3 = \frac{J_1 - J_2}{J_3}. \quad (13)$$

It is bounded by ± 1 when all heat injected by 3 is absorbed by a single terminal. However, this only occurs in chiral setups like quantum Hall edge states^{95,138,139}, as long as heat transport is avoided through the bulk.

The result is plotted in Fig. 12, where \mathcal{C}_3 changes sign around integer multiples of $\phi = \pi$, as expected from the Onsager-Casimir reciprocity relations, and around the potentials where the eigenstates cross between the two conducting diamonds B_1 and B_2 , marked by symbols in Fig. 12(a) (see also Fig. 10 and the discussion therein), forming a rhomboidal-shaped structure. This evidences that some of the circulating states do not contribute to \mathcal{C}_3 .

The circulator achieves coefficients close to 0.8 for intermediate values of the coupling. Both for strongly and very weakly coupled systems the performance is reduced. In particular, weakly coupled systems give a finite \mathcal{C}_3 only very close to $\phi = \pi$, see Fig. 12(b). This is expected, as in our case, both \mathcal{T}_{\odot}^w and \mathcal{T}_{\ominus}^w vanish simultaneously at $\phi = \pi$, see Eq. (11). Asymmetric rings will not have such constriction and are expected to improve \mathcal{C}_3 .

We compare the all-thermal and electrothermal cases in Fig. 12(b). As for the thermal switch, they have very similar behaviour, with the electrothermal device outperforming the all-thermal one, specially at low couplings. In the electrother-

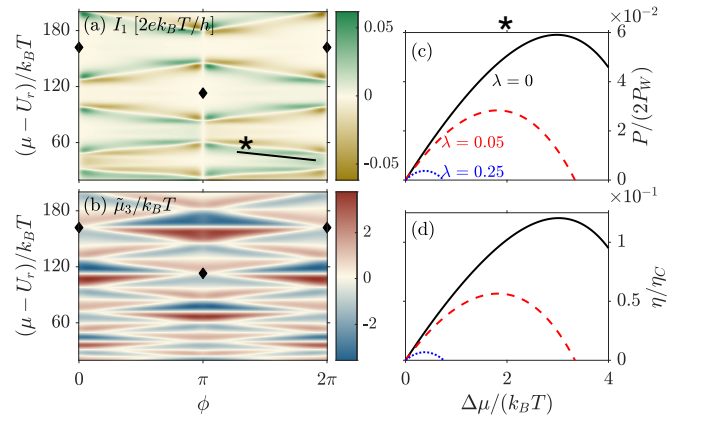


FIG. 13. (a) Generated current for $\Delta\mu = 0$, and (b) developed potential in the hot source, as a function of the magnetic flux and the internal potential in the nonlocal heat engine configuration, when reservoir 3 is at a higher temperature with $\Delta T/T = 1$. (c) Power and (d) efficiency for the configuration marked by \star (at $\phi = \pi$, $\mu - U_r = 41k_B T$) in (a), as functions of the applied voltage and in the presence of dephasing. Parameters: $\varepsilon = 0.15$, $L = l_0/2$

mal condition, we can again get analytical insight, since

$$J_1 - J_2 = \frac{2}{h} \int_{-U_r}^{\infty} dE (E - \mu) \delta\mathcal{T}(E) [f_{eq}(E) - f_3(E)], \quad (14)$$

i.e., $J_1 - J_2 \propto \sin \phi$. The sign of the circulation depends however also on the energy dependence of the kinetic phase, which needs to be integrated.

C. Nonlocal thermoelectric engine

The three-terminal setup can also be used as an energy harvester: terminal 3 is coupled to a heat source that injects a current J_3 with $I_3 = 0$. Previous works have found that this heat currents are able to induce a charge current between the other two terminals (having the same temperature T and chemical potential μ) provided the conductor has broken electron-hole and inversion symmetries^{140,141}. In coherent conductors, the electron-hole symmetry is broken by the kinetic phase⁶⁰⁻⁶⁶. Here we propose the magnetic phase to also break the inversion symmetry. The argument is simple: with $f_1 = f_2 = f_{eq}$, the elastic transport between 1 and 2 vanishes, and the charge current in the hot terminal is

$$I_3 = -I_1 - I_2 = \frac{2}{h} \int dE [\mathcal{T}_{\odot}(E) + \mathcal{T}_{\ominus}(E)] [f_3(E) - f_{eq}(E)], \quad (15)$$

with the two terms within the first pair of brackets being the contribution of the current absorbed by terminals one and two, respectively. Thus, in order to have $I_3 = 0$, the magnetoasymmetry makes it possible that a $\mu_3 = \tilde{\mu}_3$ develops so that these two contributions have equal magnitude but are opposite in sign. We write the distribution of terminal 3 at that chemical potential as \tilde{f}_3 . Hence

$$I_1 = -I_2 = \frac{2}{h} \int dE \mathcal{T}_{\odot}(E) [f_{eq}(E) - \tilde{f}_3(E)] \quad (16)$$

is the generated current that is measured between 1 and 2 (with the sign defined by the details of the transmission) via the inelastic scattering at terminal 3. The result is plotted in Fig. 13(a).

We get an intuition of the resulting current by performing a Sommerfeld expansion (valid in the linear regime at temperatures small compared with the range of variation of the transmission probabilities⁶⁶):

$$\frac{I_1}{2q_H} = \frac{\mathcal{T}_\circ(\mu, \phi)\mathcal{T}'_\circ(\mu, -\phi) - \mathcal{T}_\circ(\mu, -\phi)\mathcal{T}'_\circ(\mu, \phi)}{\mathcal{T}_\circ(\mu, \phi) + \mathcal{T}_\circ(\mu, -\phi)} \Delta T \quad (17)$$

in terms of a single transmission coefficient and its energy derivative, $\mathcal{T}'_\circ = \partial_E \mathcal{T}_\circ$, where $q_H = \pi^2 k_B^2 T / 3h$. The chemical potential developed in the hot reservoir is

$$\tilde{\mu}_3 = \mu - hq_H \frac{\mathcal{T}'_\circ(\mu, \phi) + \mathcal{T}'_\circ(\mu, -\phi)}{\mathcal{T}_\circ(\mu, \phi) + \mathcal{T}_\circ(\mu, -\phi)} \Delta T, \quad (18)$$

Note that in our symmetric configuration, at the crossing points between conducting regions [marked by diamond-shaped symbols in Fig. 9(a)], one can further simplify this expression by noticing that $\mathcal{T}_\circ(\mu, -\phi) = \mathcal{T}_\circ(\mu, \phi)$, see Fig. 9(b), hence

$$I_1 = -q_H \partial_E (\delta \mathcal{T}) \quad (19)$$

even if $\delta\mu_3 = 0$ at those conditions, see Fig. 13(b). In other words, the generated current gives a direct measure of the Onsager-Casimir reciprocity relations.

The highest values for the currents coincide with the regions where \mathcal{C}_3 is maximal (at the outer edges of the B_1 and B_2 regions, see Figs. 9(a) and 12(a)). These features emphasize the role of the magnetoasymmetry in enabling the thermoelectric effect.

Although smaller, a finite current is also generated within the insulating regions A, see for example the region marked by a star symbol. This is a consequence of having a finite temperature, which allows the nearby resonances for energies above $\mu - U_r$ for $\mathcal{T}_\circ(\mu, \phi)$ and below $\mu - U_r$ for $\mathcal{T}_\circ(\mu, \phi)$ to contribute to transport, with their derivatives contributing with the same sign to the current, cf. Eq. (19). This property, identified as the optimal condition for energy harvesting in gate controlled devices^{74,111,142} is here uniquely due to magnetic reciprocity relations. While other configurations close to $\phi = \pi$ show a larger current at $\Delta\mu = 0$ (due to narrow resonances), the cooperation of reciprocal transport coefficients at the condition marked by a star in Fig. 13(a) provides a much larger power and efficiency ($\eta = P/J_3$) at finite $\Delta\mu$, as plotted in Figs. 13(c) and 13(d).

Both the generated power and the efficiency are modest in absolute terms, see Figs. 13(c) and 13(d). However, comparing with previous interference-induced nonlocal engines with no explicit energy-dependent scattering regions⁶⁶, the nonreciprocal effect leads to a considerably enhanced thermoelectric performance. This can always be optimized by considering energy-dependent junctions with $\varepsilon(E)$ (e.g., including resonant-tunneling barriers⁷⁴) or allowing for asymmetric configurations.

V. CONCLUSIONS

We have proposed the magnetic flux through annular junctions of coherent conductors to control the thermal and thermoelectric effects via quantum interference in multiterminal devices. We consider a minimal model of a single-channel ring connected either to two or three terminals, finding that the interplay of kinetic and magnetic phases displays a rich interference pattern with sharp resonances due to the presence of circulating currents, and regions with destructive interference which can be tuned both with external gates and magnetic fields. We provide an interpretation of these features in terms of the spectral properties of the junction, in particular the symmetries of its transmission probabilities.

In two terminal configurations, the system can be used as a thermoelectric generator achieving either high efficiencies or high output power when using either very sharp peaks (in the weak coupling limit) or wider double resonances (in intermediate coupling regimes). Conditions of destructive interference which do not depend on energetic details induce a magnetic thermal switch whose efficiency remains high in the presence of dephasing.

We introduce the three terminal geometry which allows for more complex functionalities when heat is injected from the third terminal. We investigate all-thermal and electro-thermal configurations. The spatial separation of the cold terminal junctions introduces additional phases that avoid the thermal switch effect to occur for every ring potential. Nevertheless, efficient switching for intermediately coupled rings can be found for wide regions of the ring potential. The magnetic field induced nonreciprocity of the transport coefficients can be used to define a thermal circulator able to perform efficiently even in the strongly coupled regime.

The kinetic and magnetic phases are sufficient to break the electron-hole and inversion symmetries, as needed for a conductor to work as a nonlocal thermoelectric engine. We find that the Aharonov-Bohm effect enhances the performance both in terms of the output power and the efficiency, compared to three-terminal analogues using only kinetic phases⁶⁶, with optimal configurations enabled by reciprocity relations.

We have considered a symmetric configuration which emphasizes the role of quantum phases in symmetry breaking. In realistic configurations, asymmetries in the distance between junctions may compromise the occurrence of destructive interference, which can however be controlled by additional gate potentials. Exploring these asymmetries and allowing for explicitly energy-dependent scatterers may also be a way to further increase the performance of the system as a thermal circulator and converter.

ACKNOWLEDGMENTS

We thank Géraldine Haack for comments on our manuscript. We acknowledge funding from the Spanish Ministerio de Ciencia e Innovación via grants No. PID2019-110125GB-I00 and No. PID2022-142911NB-I00, and through the ‘‘María de Maeztu’’ Programme for Units of

- ¹T. T. Heikkilä, *The Physics of Nanoelectronics* (Oxford University Press, Oxford, England, UK, 2013).
- ²M. Büttiker, “Coherent and sequential tunneling in series barriers,” *IBM J. Res. Dev.* **32**, 63–75 (1988).
- ³J. C. Cuevas and E. Scheer, *Molecular Electronics* (World Scientific Publishing Company, Singapore, 2017).
- ⁴Y. Aharonov and D. Bohm, “Significance of electromagnetic potentials in the quantum theory,” *Phys. Rev.* **115**, 485–491 (1959).
- ⁵Y. Gefen, Y. Imry, and M. Y. Azbel, “Quantum Oscillations and the Aharonov-Bohm Effect for Parallel Resistors,” *Phys. Rev. Lett.* **52**, 129–132 (1984).
- ⁶M. Büttiker, Y. Imry, and M. Ya. Azbel, “Quantum oscillations in one-dimensional normal-metal rings,” *Phys. Rev. A* **30**, 1982–1989 (1984).
- ⁷R. A. Webb, S. Washburn, C. P. Umbach, and R. B. Laibowitz, “Observation of $\frac{h}{e}$ Aharonov-Bohm Oscillations in Normal-Metal Rings,” *Phys. Rev. Lett.* **54**, 2696–2699 (1985).
- ⁸S. Datta, M. R. Melloch, S. Bandyopadhyay, R. Noren, M. Vaziri, M. Müller, and R. Reifenberger, “Novel interference effects between parallel quantum wells,” *Phys. Rev. Lett.* **55**, 2344–2347 (1985).
- ⁹M. Büttiker, “Four-terminal phase-coherent conductance,” *Phys. Rev. Lett.* **57**, 1761–1764 (1986).
- ¹⁰A. D. Benoit, S. Washburn, C. P. Umbach, R. B. Laibowitz, and R. A. Webb, “Asymmetry in the magnetoconductance of metal wires and loops,” *Phys. Rev. Lett.* **57**, 1765–1768 (1986).
- ¹¹H. B. G. Casimir, “On Onsager’s Principle of Microscopic Reversibility,” *Rev. Mod. Phys.* **17**, 343–350 (1945).
- ¹²M. Büttiker, “Symmetry of electrical conduction,” *IBM J. Res. Dev.* **32**, 317–334 (1988).
- ¹³P. N. Butcher, “Thermal and electrical transport formalism for electronic microstructures with many terminals,” *J. Phys.: Condens. Matter* **2**, 4869 (1990).
- ¹⁴P. Jacquod, R. S. Whitney, J. Meair, and M. Büttiker, “Onsager relations in coupled electric, thermoelectric, and spin transport: The tenfold way,” *Phys. Rev. B* **86**, 155118 (2012).
- ¹⁵S. Nakamura, Y. Yamauchi, M. Hashisaka, K. Chida, K. Kobayashi, T. Ono, R. Leturcq, K. Ensslin, K. Saito, Y. Utsumi, and A. C. Gossard, “Nonequilibrium fluctuation relations in a quantum coherent conductor,” *Phys. Rev. Lett.* **104**, 080602 (2010).
- ¹⁶S. Nakamura, Y. Yamauchi, M. Hashisaka, K. Chida, K. Kobayashi, T. Ono, R. Leturcq, K. Ensslin, K. Saito, Y. Utsumi, and A. C. Gossard, “Fluctuation theorem and microreversibility in a quantum coherent conductor,” *Phys. Rev. B* **83**, 155431 (2011).
- ¹⁷I. L. Aleiner, N. S. Wingreen, and Y. Meir, “Dephasing and the orthogonality catastrophe in tunneling through a quantum dot: The “which path?” interferometer,” *Phys. Rev. Lett.* **79**, 3740–3743 (1997).
- ¹⁸E. Buks, R. Schuster, M. Heiblum, D. Mahalu, and V. Umansky, “Dephasing in electron interference by a ‘which-path’ detector,” *Nature* **391**, 871–874 (1998).
- ¹⁹A. Yacoby, M. Heiblum, D. Mahalu, and H. Shtrikman, “Coherence and phase sensitive measurements in a quantum dot,” *Phys. Rev. Lett.* **74**, 4047–4050 (1995).
- ²⁰A. Levy Yeyati and M. Büttiker, “Aharonov-Bohm oscillations in a mesoscopic ring with a quantum dot,” *Phys. Rev. B* **52**, R14360–R14363 (1995).
- ²¹G. Hackenbroich and H. A. Weidenmüller, “Transmission through a Quantum Dot in an Aharonov-Bohm Ring,” *Phys. Rev. Lett.* **76**, 110–113 (1996).
- ²²Y. Oreg and Y. Gefen, “Electron scattering through a quantum dot: A phase lapse mechanism,” *Phys. Rev. B* **55**, 13726–13729 (1997).
- ²³C. Bruder, R. Fazio, and H. Schoeller, “Aharonov-Bohm Oscillations and Resonant Tunneling in Strongly Correlated Quantum Dots,” *Phys. Rev. Lett.* **76**, 114–117 (1996).
- ²⁴A. Yacoby, M. Heiblum, D. Mahalu, and H. Shtrikman, “Coherence and phase sensitive measurements in a quantum dot,” *Solid-State Electron.* **40**, 225–231 (1996).
- ²⁵R. Schuster, E. Buks, M. Heiblum, D. Mahalu, V. Umansky, and H. Shtrikman, “Phase measurement in a quantum dot via a double-slit interference experiment,” *Nature* **385**, 417–420 (1997).
- ²⁶G. Cernicchiaro, T. Martin, K. Hasselbach, D. Mailly, and A. Benoit, “Channel Interference in a Quasiballistic Aharonov-Bohm Experiment,” *Phys. Rev. Lett.* **79**, 273–276 (1997).
- ²⁷K. Kobayashi, H. Aikawa, S. Katsumoto, and Y. Iye, “Tuning of the Fano Effect through a Quantum Dot in an Aharonov-Bohm Interferometer,” *Phys. Rev. Lett.* **88**, 256806 (2002).
- ²⁸K. Kobayashi, H. Aikawa, S. Katsumoto, and Y. Iye, “Mesoscopic Fano effect in a quantum dot embedded in an Aharonov-Bohm ring,” *Phys. Rev. B* **68**, 235304 (2003).
- ²⁹M. Sigrist, A. Fuhrer, T. Ihn, K. Ensslin, S. E. Ulloa, W. Wegscheider, and M. Bichler, “Magnetic-field-dependent transmission phase of a double-dot system in a quantum ring,” *Phys. Rev. Lett.* **93**, 066802 (2004).
- ³⁰K. Kobayashi, H. Aikawa, A. Sano, S. Katsumoto, and Y. Iye, “Fano resonance in a quantum wire with a side-coupled quantum dot,” *Phys. Rev. B* **70**, 035319 (2004).
- ³¹M. Avinun-Kalish, M. Heiblum, O. Zarchin, D. Mahalu, and V. Umansky, “Crossover from ‘mesoscopic’ to ‘universal’ phase for electron transmission in quantum dots,” *Nature* **436**, 529–533 (2005).
- ³²S. S. Buchholz, S. F. Fischer, U. Kunze, M. Bell, D. Reuter, and A. D. Wieck, “Control of the transmission phase in an asymmetric four-terminal aharonov-bohm interferometer,” *Phys. Rev. B* **82**, 045432 (2010).
- ³³S. S. Buchholz, E. Sternemann, O. Chiatti, D. Reuter, A. D. Wieck, and S. F. Fischer, “Noise thermometry in narrow two-dimensional electron gas heat baths connected to a quasi-one-dimensional interferometer,” *Phys. Rev. B* **85**, 235301 (2012).
- ³⁴G. Behner, A. R. Jalil, D. Heffels, J. Kölzer, K. Moors, J. Mertens, E. Zimmermann, G. Mussler, P. Schüffelgen, H. Lüth, D. Grützmacher, and T. Schäpers, “Aharonov-Bohm Interference and Phase-Coherent Surface-State Transport in Topological Insulator Rings,” *Nano Lett.* **23**, 6347–6353 (2023).
- ³⁵S. Biswas, H. K. Kundu, R. Bhattacharyya, V. Umansky, and M. Heiblum, “Anomalous Aharonov-Bohm interference in the presence of edge reconstruction,” *Phys. Rev. Lett.* **132**, 076301 (2024).
- ³⁶J. Kim, H. Dev, R. Kumar, A. Ilin, A. Haug, V. Bhardwaj, C. Hong, K. Watanabe, T. Taniguchi, A. Stern, and Y. Ronen, “Aharonov-Bohm interference and the evolution of phase jumps in fractional quantum Hall Fabry-Perot interferometers based on bi-layer graphene,” *arXiv* (2024), 2402.12432.
- ³⁷W. Hofstetter, J. König, and H. Schoeller, “Kondo Correlations and the Fano Effect in Closed Aharonov-Bohm Interferometers,” *Phys. Rev. Lett.* **87**, 156803 (2001).
- ³⁸O. Entin-Wohlman, A. Aharony, Y. Imry, and Y. Levinson, “The Fano Effect in Aharonov-Bohm Interferometers,” *J. Low Temp. Phys.* **126**, 1251–1273 (2002).
- ³⁹B. Kubala and J. König, “Aharonov-bohm interferometry with quantum dots: scattering approach versus tunneling picture,” *Phys. Rev. B* **67**, 205303 (2003).
- ⁴⁰Z.-B. He and Y.-J. Xiong, “Electron transport through an Aharonov–Bohm ring with a side-coupled quantum dot,” *Phys. Lett. A* **349**, 276–280 (2006).
- ⁴¹C. Emary, “Dark states in the magnetotransport through triple quantum dots,” *Phys. Rev. B* **76**, 245319 (2007).
- ⁴²D. Rai, O. Hod, and A. Nitzan, “Magnetic fields effects on the electronic conduction properties of molecular ring structures,” *Phys. Rev. B* **85**, 155440 (2012).
- ⁴³S. Bedkhal, M. Bandyopadhyay, and D. Segal, “Flux-dependent occupations and occupation difference in geometrically symmetric and energy degenerate double-dot aharonov-bohm interferometers,” *Phys. Rev. B* **87**, 045418 (2013).
- ⁴⁴B. D’Anjou and W. A. Coish, “Anomalous magnetotransport through reflection-symmetric artificial molecules,” *Phys. Rev. B* **87**, 085443 (2013).
- ⁴⁵J. Lu, Y. Liu, R. Wang, C. Wang, and J.-H. Jiang, “Optimal efficiency and power, and their trade-off in three-terminal quantum thermoelectric engines with two output electric currents,” *Phys. Rev. B* **100**, 115438 (2019).
- ⁴⁶U. Sivan and Y. Imry, “Multichannel Landauer formula for thermoelectric transport with application to thermopower near the mobility edge,” *Phys. Rev. B* **33**, 551–558 (1986).
- ⁴⁷M. Paulsson and S. Datta, “Thermoelectric effect in molecular electronics,” *Phys. Rev. B* **67**, 241403 (2003).
- ⁴⁸C. M. Finch, V. M. García-Suárez, and C. J. Lambert, “Giant thermopower and figure of merit in single-molecule devices,” *Phys. Rev. B* **79**, 033405

- (2009).
- ⁴⁹J. P. Bergfield and C. A. Stafford, “Thermoelectric Signatures of Coherent Transport in Single-Molecule Heterojunctions,” *Nano Lett.* **9**, 3072–3076 (2009).
- ⁵⁰O. Karlström, H. Linke, G. Karlström, and A. Wacker, “Increasing thermoelectric performance using coherent transport,” *Phys. Rev. B* **84**, 113415 (2011).
- ⁵¹P. Trocha and J. Barnaś, “Large enhancement of thermoelectric effects in a double quantum dot system due to interference and Coulomb correlation phenomena,” *Phys. Rev. B* **85**, 085408 (2012).
- ⁵²G. Gómez-Silva, O. Ávalos Ovando, M. L. Ladrón de Guevara, and P. A. Orellana, “Enhancement of thermoelectric efficiency and violation of the Wiedemann-Franz law due to Fano effect,” *J. Appl. Phys.* **111**, 053704 (2012).
- ⁵³S. Hershfield, K. A. Muttalib, and B. J. Nartowt, “Nonlinear thermoelectric transport: A class of nanodevices for high efficiency and large power output,” *Phys. Rev. B* **88**, 085426 (2013).
- ⁵⁴N. Nakpathomkun, H. Q. Xu, and H. Linke, “Thermoelectric efficiency at maximum power in low-dimensional systems,” *Phys. Rev. B* **82**, 235428 (2010).
- ⁵⁵L. Rincón-García, A. K. Ismael, C. Evangeli, I. Grace, G. Rubio-Bollinger, K. Porfyrakis, N. Agrait, and C. J. Lambert, “Molecular design and control of fullerene-based bi-thermoelectric materials,” *Nat. Mater.* **15**, 289–293 (2016).
- ⁵⁶L. Cui, R. Miao, K. Wang, D. Thompson, L. A. Zotti, J. C. Cuevas, E. Meyhofer, and P. Reddy, “Peltier cooling in molecular junctions,” *Nat. Nanotechnol.* **13**, 122–127 (2017).
- ⁵⁷R. Miao, H. Xu, M. Skripnik, L. Cui, K. Wang, K. G. L. Pedersen, M. Leijnse, F. Pauly, K. Wärmarm, E. Meyhofer, P. Reddy, and H. Linke, “Influence of Quantum Interference on the Thermoelectric Properties of Molecular Junctions,” *Nano Lett.* **18**, 5666–5672 (2018).
- ⁵⁸B. Brun, F. Martins, S. Faniel, A. Cavanna, C. Ulysse, A. Ouerghi, U. Gennser, D. Mailly, P. Simon, S. Huant, M. Sanquer, H. Sellier, V. Bayot, and B. Hackens, “Thermoelectric scanning-gate interferometry on a quantum point contact,” *Phys. Rev. Applied* **11**, 034069 (2019).
- ⁵⁹J. M. Hamill, A. Ismael, A. Al-Jobory, T. L. R. Bennett, M. Alshahrani, X. Wang, M. Akers-Douglas, L. A. Wilkinson, B. J. Robinson, N. J. Long, C. Lambert, and T. Albrecht, “Quantum Interference and Contact Effects in the Thermoelectric Performance of Anthracene-Based Molecules,” *J. Phys. Chem. C* **127**, 7484–7491 (2023).
- ⁶⁰P. P. Hofer and B. Sothmann, “Quantum heat engines based on electronic Mach-Zehnder interferometers,” *Phys. Rev. B* **91**, 195406 (2015).
- ⁶¹L. Vannucci, F. Ronetti, G. Dolcetto, M. Carrega, and M. Sassetti, “Interference-induced thermoelectric switching and heat rectification in quantum Hall junctions,” *Phys. Rev. B* **92**, 075446 (2015).
- ⁶²P. Samuelsson, S. Kheradsoud, and B. Sothmann, “Optimal Quantum Interference Thermoelectric Heat Engine with Edge States,” *Phys. Rev. Lett.* **118**, 256801 (2017).
- ⁶³G. Haack and F. Giazotto, “Efficient and tunable Aharonov-Bohm quantum heat engine,” *Phys. Rev. B* **100**, 235442 (2019).
- ⁶⁴G. Haack and F. Giazotto, “Nonlinear regime for enhanced performance of an Aharonov-Bohm heat engine,” *AVS Quantum Sci.* **3**, 046801 (2021).
- ⁶⁵G. Fleury, C. Gorini, and R. Sánchez, “Scanning probe-induced thermoelectrics in a quantum point contact,” *Appl. Phys. Lett.* **119**, 043101 (2021).
- ⁶⁶R. Sánchez, C. Gorini, and G. Fleury, “Extrinsic thermoelectric response of coherent conductors,” *Phys. Rev. B* **104**, 115430 (2021).
- ⁶⁷G. Blasi, F. Giazotto, and G. Haack, “Hybrid normal-superconducting Aharonov-Bohm quantum thermal device,” *Quantum Sci. Technol.* **8**, 015023 (2022).
- ⁶⁸O. Entin-Wohlman, Y. Imry, and A. Aharony, “Three-terminal thermoelectric transport through a molecular junction,” *Phys. Rev. B* **82**, 115314 (2010).
- ⁶⁹R. Sánchez and M. Büttiker, “Optimal energy quanta to current conversion,” *Phys. Rev. B* **83**, 085428 (2011).
- ⁷⁰D. Sánchez and L. Serra, “Thermoelectric transport of mesoscopic conductors coupled to voltage and thermal probes,” *Phys. Rev. B* **84**, 201307 (2011).
- ⁷¹O. Entin-Wohlman and A. Aharony, “Three-terminal thermoelectric transport under broken time-reversal symmetry,” *Phys. Rev. B* **85**, 085401 (2012).
- ⁷²F. Mazza, R. Bosisio, G. Benenti, V. Giovannetti, R. Fazio, and F. Taddei, “Thermoelectric efficiency of three-terminal quantum thermal machines,” *New J. Phys.* **16**, 085001 (2014).
- ⁷³F. Mazza, S. Valentini, R. Bosisio, G. Benenti, V. Giovannetti, R. Fazio, and F. Taddei, “Separation of heat and charge currents for boosted thermoelectric conversion,” *Phys. Rev. B* **91**, 245435 (2015).
- ⁷⁴J. Balduque and R. Sánchez, “Coherent control of thermoelectric currents and noise in quantum thermocouples,” *Phys. Rev. B* **109**, 045429 (2024).
- ⁷⁵Y. Dubi and M. Di Ventra, “Colloquium: Heat flow and thermoelectricity in atomic and molecular junctions,” *Rev. Mod. Phys.* **83**, 131–155 (2011).
- ⁷⁶G. Benenti, G. Casati, K. Saito, and R. S. Whitney, “Fundamental aspects of steady-state conversion of heat to work at the nanoscale,” *Phys. Rep.* **694**, 1 (2017).
- ⁷⁷D. Zhang, X. Zheng, and M. Di Ventra, “Local temperatures out of equilibrium,” *Phys. Rep.* **830**, 1–66 (2019).
- ⁷⁸F. Giazotto, T. T. Heikkilä, A. Luukanen, A. M. Savin, and J. P. Pekola, “Opportunities for mesoscopics in thermometry and refrigeration: Physics and applications,” *Rev. Mod. Phys.* **78**, 217 (2006).
- ⁷⁹C. Riha, O. Chiatti, S. S. Buchholz, D. Reuter, A. D. Wieck, and S. F. Fischer, “Heat flow, transport and fluctuations in etched semiconductor quantum wire structures,” *Phys. Status Solidi A* **213**, 571–581 (2016).
- ⁸⁰J. P. Pekola and B. Karimi, “Colloquium: Quantum heat transport in condensed matter systems,” *Rev. Mod. Phys.* **93**, 041001 (2021).
- ⁸¹D. Majidi, J. P. Bergfield, V. Maisi, J. Höfer, H. Courtois, and C. B. Winkelmann, “Heat transport at the nanoscale and ultralow temperatures—Implications for quantum technologies,” *Appl. Phys. Lett.* **124**, 140504 (2024).
- ⁸²F. Giazotto and M. J. Martínez-Pérez, “The Josephson heat interferometer,” *Nature* **492**, 401–405 (2012).
- ⁸³M. J. Martínez-Pérez, A. Fornieri, and F. Giazotto, “Rectification of electronic heat current by a hybrid thermal diode,” *Nat. Nanotechnol.* **10**, 303–307 (2015).
- ⁸⁴A. Ronzani, B. Karimi, J. Senior, Y.-C. Chang, J. T. Peltonen, C. Chen, and J. P. Pekola, “Tunable photonic heat transport in a quantum heat valve,” *Nat. Phys.* **14**, 991–995 (2018).
- ⁸⁵J. Senior, A. Gubaydullin, B. Karimi, J. T. Peltonen, J. Ankerhold, and J. P. Pekola, “Heat rectification via a superconducting artificial atom,” *Commun. Phys.* **3**, 40 (2020).
- ⁸⁶A. Gubaydullin, G. Thomas, D. S. Golubev, D. Lvov, J. T. Peltonen, and J. P. Pekola, “Photonic heat transport in three terminal superconducting circuit,” *Nat. Commun.* **13**, 1–10 (2022).
- ⁸⁷D. Subero, O. Maillet, D. S. Golubev, G. Thomas, J. T. Peltonen, B. Karimi, M. Marín-Suárez, A. L. Yeyati, R. Sánchez, S. Park, and J. P. Pekola, “Bolometric detection of Josephson inductance in a highly resistive environment,” *Nat. Commun.* **14**, 1–8 (2023).
- ⁸⁸S. Jezouin, F. D. Parmentier, A. Anthore, U. Gennser, A. Cavanna, Y. Jin, and F. Pierre, “Quantum Limit of Heat Flow Across a Single Electronic Channel,” *Science* **342**, 601–604 (2013).
- ⁸⁹H. Thierschmann, F. Arnold, M. Mittermüller, L. Maier, C. Heyn, W. Hansen, H. Buhmann, and L. W. Molenkamp, “Thermal gating of charge currents with Coulomb coupled quantum dots,” *New J. Phys.* **17**, 113003 (2015).
- ⁹⁰B. Dutta, J. T. Peltonen, D. S. Antonenko, M. Meschke, M. A. Skvortsov, B. Kubala, J. König, C. B. Winkelmann, H. Courtois, and J. P. Pekola, “Thermal conductance of a single-electron transistor,” *Phys. Rev. Lett.* **119**, 077701 (2017).
- ⁹¹B. Karimi, J. P. Pekola, M. Campisi, and R. Fazio, “Coupled qubits as a quantum heat switch,” *Quantum Sci. Technol.* **2**, 044007 (2017).
- ⁹²D. Goury and R. Sánchez, “Reversible thermal diode and energy harvester with a superconducting quantum interference single-electron transistor,” *Appl. Phys. Lett.* **115**, 092601 (2019).
- ⁹³N. S. Kirsanov, Z. B. Tan, D. S. Golubev, P. J. Hakonen, and G. B. Lesovik, “Heat switch and thermoelectric effects based on Cooper-pair splitting and elastic cotunneling,” *Phys. Rev. B* **99**, 115127 (2019).
- ⁹⁴S.-Y. Hwang, B. Sothmann, and R. López, “Phase-controlled heat modulation with Aharonov-Bohm interferometers,” *Phys. Rev. Res.* **6**, 013215 (2024).
- ⁹⁵R. Sánchez, B. Sothmann, and A. N. Jordan, “Heat diode and engine based on quantum Hall edge states,” *New J. Phys.* **17**, 075006 (2015).

- ⁹⁶S.-Y. Hwang, F. Giazotto, and B. Sothmann, “Phase-Coherent Heat Circulator Based on Multiterminal Josephson Junctions,” *Phys. Rev. Appl.* **10**, 044062 (2018).
- ⁹⁷M. Acciai, F. Hajiloo, F. Hassler, and J. Splettstoesser, “Phase-coherent heat circulators with normal or superconducting contacts,” *Phys. Rev. B* **103**, 085409 (2021).
- ⁹⁸I. Díaz and R. Sánchez, “The qutrit as a heat diode and circulator,” *New J. Phys.* **23**, 125006 (2021).
- ⁹⁹L. Wang and B. Li, “Thermal logic gates: Computation with phonons,” *Phys. Rev. Lett.* **99**, 177208 (2007).
- ¹⁰⁰D. Segal, “Nonlinear thermal control in an n -terminal junction,” *Phys. Rev. E* **77**, 021103 (2008).
- ¹⁰¹N. Li, J. Ren, L. Wang, G. Zhang, P. Hänggi, and B. Li, “Colloquium: Phononics: Manipulating heat flow with electronic analogs and beyond,” *Rev. Mod. Phys.* **84**, 1045–1066 (2012).
- ¹⁰²M. Tsaousidou and G. P. Triberis, “Thermal conductance of a weakly coupled quantum dot,” *AIP Conf. Proc.* **893**, 801–802 (2007).
- ¹⁰³X. Zianni, “Coulomb oscillations in the electron thermal conductance of a dot in the linear regime,” *Phys. Rev. B* **75**, 045344 (2007).
- ¹⁰⁴B. Kubala, J. König, and J. Pekola, “Violation of the wiedemann-franz law in a single-electron transistor,” *Phys. Rev. Lett.* **100**, 066801 (2008).
- ¹⁰⁵G. D. Guttman, E. Ben-Jacob, and D. J. Bergman, “Thermopower of mesoscopic and disordered systems,” *Phys. Rev. B* **51**, 17758–17766 (1995).
- ¹⁰⁶Y. M. Blanter, C. Bruder, R. Fazio, and H. Schoeller, “Aharonov-Bohm-type oscillations of thermopower in a quantum-dot ring geometry,” *Phys. Rev. B* **55**, 4069–4072 (1997).
- ¹⁰⁷X. Lu, J.-S. Wang, W. G. Morrel, X. Ni, C.-Q. Wu, and B. Li, “Thermoelectric effect in Aharonov–Bohm structures,” *J. Phys.: Condens. Matter* **27**, 035301 (2014).
- ¹⁰⁸H. Thierschmann, R. Sánchez, B. Sothmann, F. Arnold, C. Heyn, W. Hansen, H. Buhmann, and L. W. Molenkamp, “Three-terminal energy harvester with coupled quantum dots,” *Nat. Nanotechnol.* **10**, 854 (2015).
- ¹⁰⁹B. Roche, P. Rouleau, T. Jullien, Y. Jompol, I. Farrer, D. A. Ritchie, and D. C. Glattli, “Harvesting dissipated energy with a mesoscopic ratchet,” *Nat. Commun.* **6**, 6738 (2015).
- ¹¹⁰F. Hartmann, P. Pfeffer, S. Höfling, M. Kamp, and L. Worschech, “Voltage fluctuation to current converter with Coulomb-coupled quantum dots,” *Phys. Rev. Lett.* **114**, 146805 (2015).
- ¹¹¹A. N. Jordan, B. Sothmann, R. Sánchez, and M. Büttiker, “Powerful and efficient energy harvester with resonant-tunneling quantum dots,” *Phys. Rev. B* **87**, 075312 (2013).
- ¹¹²G. Jaliel, R. K. Puddy, R. Sánchez, A. N. Jordan, B. Sothmann, I. Farrer, J. P. Griffiths, D. A. Ritchie, and C. G. Smith, “Experimental realization of a quantum dot energy harvester,” *Phys. Rev. Lett.* **123**, 117701 (2019).
- ¹¹³S. Dorsch, A. Svilans, M. Josefsson, B. Goldozian, M. Kumar, C. Thelander, A. Wacker, and A. Burke, “Heat Driven Transport in Serial Double Quantum Dot Devices,” *Nano Lett.* **21**, 988–994 (2021).
- ¹¹⁴S. Dorsch, S. Fahlvik, and A. Burke, “Characterization of electrostatically defined bottom-heated InAs nanowire quantum dot systems,” *New J. Phys.* **23**, 125007 (2021).
- ¹¹⁵W. Khan, P. P. Potts, S. Lehmann, C. Thelander, K. A. Dick, P. Samuelsson, and V. F. Maisi, “Efficient and continuous microwave photoconversion in hybrid cavity-semiconductor nanowire double quantum dot diodes,” *Nat. Commun.* **12**, 1–7 (2021).
- ¹¹⁶S. Haldar, D. Zenelaj, P. P. Potts, H. Havir, S. Lehmann, K. A. Dick, P. Samuelsson, and V. F. Maisi, “Microwave power harvesting using resonator-coupled double quantum dot photodiode,” *Phys. Rev. B* **109**, L081403 (2024).
- ¹¹⁷M. Büttiker, “Role of quantum coherence in series resistors,” *Phys. Rev. B* **33**, 3020–3026 (1986).
- ¹¹⁸M. J. M. de Jong and C. W. J. Beenakker, “Semiclassical theory of shot noise in mesoscopic conductors,” *Physica A* **230**, 219–248 (1996).
- ¹¹⁹M. Büttiker, Y. Imry, and R. Landauer, “Josephson behavior in small normal one-dimensional rings,” *Phys. Lett. A* **96**, 365–367 (1983).
- ¹²⁰T. Ihn, *Semiconductor Nanostructures: Quantum states and electronic transport* (Oxford University Press, 2009).
- ¹²¹S. Datta, *Electronic Transport in Mesoscopic Systems* (Cambridge University Press, 1995).
- ¹²²M. V. Moskalets, *Scattering Matrix Approach to Non-Stationary Quantum Transport* (Imperial College Press, 2011).
- ¹²³K. Saito, G. Benenti, G. Casati, and T. c. v. Prosen, “Thermopower with broken time-reversal symmetry,” *Phys. Rev. B* **84**, 201306 (2011).
- ¹²⁴S. Bedkhal, M. Bandyopadhyay, and D. Segal, “The probe technique far from equilibrium: Magnetic field symmetries of nonlinear transport,” *Eur. Phys. J. B* **86**, 506–18 (2013).
- ¹²⁵G. D. Mahan and J. O. Sofo, “The best thermoelectric,” *Proc. Natl. Acad. Sci. USA* **93**, 7436–7439 (1996).
- ¹²⁶R. S. Whitney, “Most Efficient Quantum Thermoelectric at Finite Power Output,” *Phys. Rev. Lett.* **112**, 130601 (2014).
- ¹²⁷J. Behera, S. Bedkhal, B. K. Agarwalla, and M. Bandyopadhyay, “Quantum coherent control of nonlinear thermoelectric transport in a triple-dot Aharonov-Bohm heat engine,” *Phys. Rev. B* **108**, 165419 (2023).
- ¹²⁸A. A. M. Staring, L. W. Molenkamp, B. W. Alphenaar, H. van Houten, O. J. A. Buyk, M. A. A. Mabeoone, C. W. J. Beenakker, and C. T. Foxon, “Coulomb-Blockade Oscillations in the Thermopower of a Quantum Dot,” *EPL* **22**, 57–62 (1993).
- ¹²⁹A. S. Dzurak, C. G. Smith, M. Pepper, D. A. Ritchie, J. E. F. Frost, G. A. C. Jones, and D. G. Hasko, “Observation of Coulomb blockade oscillations in the thermopower of a quantum dot,” *Solid State Commun.* **87**, 1145–1149 (1993).
- ¹³⁰A. S. Dzurak, C. G. Smith, C. H. W. Barnes, M. Pepper, L. Martín-Moreno, C. T. Liang, D. A. Ritchie, and G. A. C. Jones, “Thermoelectric signature of the excitation spectrum of a quantum dot,” *Phys. Rev. B* **55**, R10197–R10200(R) (1997).
- ¹³¹R. Scheibner, E. G. Novik, T. Borzenko, M. König, D. Reuter, A. D. Wieck, H. Buhmann, and L. W. Molenkamp, “Sequential and cotunneling behavior in the temperature-dependent thermopower of few-electron quantum dots,” *Phys. Rev. B* **75**, 041301 (2007).
- ¹³²S. F. Svensson, A. I. Persson, E. A. Hoffmann, N. Nakpathomkun, H. A. Nilsson, H. Q. Xu, L. Samuelson, and H. Linke, “Lineshape of the thermopower of quantum dots,” *New J. Phys.* **14**, 033041 (2012).
- ¹³³S. F. Svensson, E. A. Hoffmann, N. Nakpathomkun, P. M. Wu, H. Q. Xu, H. A. Nilsson, D. Sánchez, V. Kashcheyevs, and H. Linke, “Non-linear thermovoltage and thermocurrent in quantum dots,” *New J. Phys.* **15**, 105011 (2013).
- ¹³⁴M. Josefsson, A. Svilans, A. M. Burke, E. A. Hoffmann, S. Fahlvik, C. Thelander, M. Leijnse, and H. Linke, “A quantum-dot heat engine operating close to the thermodynamic efficiency limits,” *Nat. Nanotechnol.* **13**, 920–924 (2018).
- ¹³⁵J. B. Pendry, “Quantum limits to the flow of information and entropy,” *J. Phys. A: Math. Gen.* **16**, 2161–2171 (1983).
- ¹³⁶R. S. Whitney, “Finding the quantum thermoelectric with maximal efficiency and minimal entropy production at given power output,” *Phys. Rev. B* **91**, 115425 (2015).
- ¹³⁷We have confirmed that all diamonds are insulating for J_3 when $L_c = 0$, and that sequences of M diamonds with $M - 1$ being conducting appear when $L_c = L/M$, in both cases with and $L_a = L_b = (L - L_c)/2$.
- ¹³⁸G. Granger, J. P. Eisenstein, and J. L. Reno, “Observation of chiral heat transport in the quantum Hall regime,” *Phys. Rev. Lett.* **102**, 086803 (2009).
- ¹³⁹S.-G. Nam, E. H. Hwang, and H.-J. Lee, “Thermoelectric detection of chiral heat transport in graphene in the quantum Hall regime,” *Phys. Rev. Lett.* **110**, 226801 (2013).
- ¹⁴⁰B. Sothmann, R. Sánchez, and A. N. Jordan, “Thermoelectric energy harvesting with quantum dots,” *Nanotechnology* **26**, 032001 (2015).
- ¹⁴¹R. Wang, C. Wang, J. Lu, and J.-H. Jiang, “Inelastic thermoelectric transport and fluctuations in mesoscopic systems,” *Advances in Physics: X* **7**, 2082317 (2022).
- ¹⁴²R. S. Whitney, “Quantum coherent three-terminal thermoelectrics: Maximum efficiency at given power output,” *Entropy* **18**, 208 (2016).